FORMATION AND DESTRUCTION OF SHORELINE SAND WAVES: OBSERVATIONS AND MODELLING

Jaime Arriaga[1], Albert Falques[2], Francesca Ribas[3] and Eddie Crews[4]

Abstract

The role of the high-angle wave instability mechanism in the formation of shoreline undulations observed in the northern flank of the Dungeness Cuspate Foreland (U.K.) is investigated with a linear stability model. The geographic site characteristics and the restrictions of the model require that waves are previously propagated from the wave buoy to 4 m depth, in front of the undulations. The wave climate is bimodal with oblique waves (which are supposed to be destabilizing) from the SW and nearly normal waves (which are supposed to be stabilizing) from the NE. Despite waves are propagated to a shallow depth, the incoming SW waves are still very oblique with respect to the local shoreline (above 70°) due to the shape of the cuspate foreland. The results of the stability analysis indicate that such highly-oblique waves can trigger the formation of undulations with wavelengths comparable to the observed one.

Key words: shoreline sand waves, shoreline instability, self-organization, alongshore sediment transport, Dungeness

1. Introduction

Alongshore rhythmic morphological patterns at different length scales are quite common along sandy and gravel beaches. Well-known examples are mega-cusps and crescentic bars/rip channel systems with alongshore wavelengths of the order of 1-50 m and 100-1000 m, respectively (Coco and Murray, 2007; Ribas et al., 2015; and references therein). At larger scales (wavelengths of the order of 1-10 km or more) there are the km-scale shoreline sand waves (KSSW), which are neither linked to these smaller scale patterns nor directly related to surf-zone dynamics (Verhagen, 1989; Davidson-Arnott and van Heyningen, 2003; Ryabchuk et al., 2011; Kaergaard et al., 2012). It is important to stress that the alongshore wavelength of KSSW depend on the environmental characteristics of the site and that they can be significantly reduced, e.g., to a few hundred meters, in low-energy beaches (Medellín et al., 2008).

During the last two decades there has been much research to unravel the origin of such intriguing alongshore rhythmic coastal patterns and to get insight into their dynamics. The hypothesis that they are self-organized and emerge out of positive feedbacks between hydrodynamics and morphology has been amply confirmed by mathematical modelling (Coco and Murray, 2007; Ribas et al., 2015). In particular, the potential role of high-angle wave incidence (HAWI) in driving KSSW has been investigated (Ashton et al., 2001; Falqués and Calvete, 20015; van den Berg et al., 2012; Kaergaard et al., 2013). This instability results from the feedback between nearshore bathymetric changes and the wave field, which experiences alongshore variations in the wave angle and height at breaking (the latter being due to wave energy spreading). If the wave angle is greater than a critical angle of about 45° at the depth of closure, the variations in wave height dominate and lead to transport gradients that make the perturbation grow. However, the large spatial and temporal scales of the emerging patterns have proven a major constraint to contrast the hypothesis with nature. This is so because these tests would require detailed measurements of the bathymetry and the wave conditions at the moment of their formation from a featureless morphology, whilst in most cases observations report already fully-formed KSSW. To our knowledge, such detailed data

---

[1]Department of Physics, Universitat Politècnica de Catalunya, Barcelona, Spain. jaime.alonso.arriaga@upc.edu
[2]Department of Physics, Universitat Politècnica de Catalunya, Barcelona, Spain. albert.falques@upc.edu
[3]Department of Physics, Universitat Politècnica de Catalunya, Barcelona, Spain. francesca.ribas@upc.edu
[4]WSP-Parsons Brinckerhoff, Exeter, UK. eddie.crews@wspgroup.com

during pattern formation are not reported in the literature, with the exception of the Santander spit case (Medellín et al., 2008).

Large-scale cuspate forelands and cuspate spits are coastal patterns occurring worldwide that could also be generated by HAWI (Ashton et al., 2006a,b) and, at the same time, they can house smaller-scale shoreline undulations in one of the flanks (e.g., Long Point spit in Lake Eyre, U.S.A., see Davidson-Arnott and van Heyningen, 2003). Arriaga et al. (2017a) reported detailed observations of two events of formation of shoreline undulations with a wavelength of about 400 m at the northern flank of the Dungeness Cuspate Foreland (U.K.). Despite the fact that such wavelengths are smaller than those of most of the KSSW studied previously, some studies suggest that such wavelengths are possible both in theory and in nature (Medellín et al., 2008). Arriaga et al. (2017a) also described in detail the wave conditions and bathymetric characteristics during the formation of the undulations and found a high correlation between wave obliquity and the formation events.

The aim of this contribution is to explore the role of the HAWI mechanism in the formation of the undulations in the northern flank of the Dungeness Foreland using a morphodynamic model. The observations are first presented in section 2. The morphodynamic model used requires the wave conditions in front of the undulations so that waves are first propagated across a large scale bathymetry from the deep water wave buoy to a location in front of the undulations (section 3). Also, we divide the measured wave climate in two bins: South-West (oblique waves) and North-East (nearly normal waves). Then, we use linear stability analysis to obtain the fastest growing wavelengths corresponding to the measured profile and to the two types of propagated waves (section 4). Finally, the results are discussed in section 5 and the most important conclusions are listed in section 6.

2. Observations of shoreline undulations

2.1. *Site description*

Dungeness is the largest cuspate foreland located in the southern English shore (Figure 1, left). The studied area is the 2 km long coastline at the northern flank of the foreland, which has a mean shoreline orientation of 163° with respect to North. The sediment can be classified as gravel with a mean grain size ranging from 8 mm to 150 mm (Green, 1968). However, the mean grain size is thinner in our area of interest with a range between 10 mm and 20 mm (Science report: beach material properties, 2005). The averaged intertidal beach slope in this area is 0.08, consistently with the large grain size. The slope of the cross-shore profile is largest at the tip of the cape and decreases northward. As can be seen in Figure 2 (right), the three shown profiles display a strong slope change at a certain depth.

The averaged tidal range at Dungeness is 6.7 m and the mean high water during spring tides is 4.0 m (Long et al., 2006). The role of tides is ignored in the present contribution and we focus solely in the role of waves, since they have been shown to be the main driving force for littoral drift. The wave climate is extracted from a wave buoy at 43 m depth located in front of Hastings during the period from 2006 to 2015. The wave rose (Figure 1, right) shows two dominant directions, from the South-West and from the North-East, the former is more energetic and occur 65% of the time. The averaged wave conditions (corresponding to the SW and NE waves) are $\bar{H}_{SW} = 1.4$ m, $\bar{T}_{SW} = 6.8$ s, $\bar{\varphi}_{SW} = 234^o$ and $\bar{H}_{NE} = 0.93$ m, $\bar{T}_{NE} = 5.5$ s, $\bar{\varphi}_{NE} = 66^o$ (angles with respect to the north). The mean wave height is computed with a power 5/2 because, according to the well-known CERC formula, the total alongshore sediment transport rate is proportional to $H^{5/2}$. Also, the wave period and angle are averaged with a weight of $H^{5/2}$.
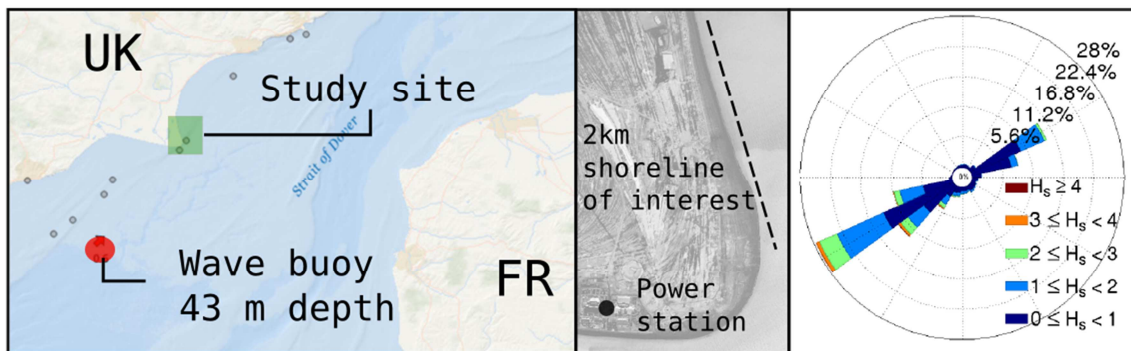
Figure 1. Location map of the study site and the wave buoy (left; image modified from the Channel Coastal Observatory). Zoom of the area of interest is shown (centre; image modified from Google Earth and corresponds to September 2013). Wave rose for the period 2006-2015 (right).

2.2. *Shoreline undulations*

Arriaga et al. (2017a) described events of formation and destruction of shoreline undulations with alongshore wavelengths of 350-450~m along the northern flank of the Dungeness Foreland, near the tip, using topographic intertidal measurements of two types: survey profiles performed every three months and one annual topographic survey with a high alongshore resolution. On February 2007, KSSW were formed and they were destroyed in 2009. Another formation event occurred on July 2014 and these undulations still persisted in February 2016 (the end of the study period) and had migrated northward at a mean rate of about 200 m/yr (Figure 2, left).
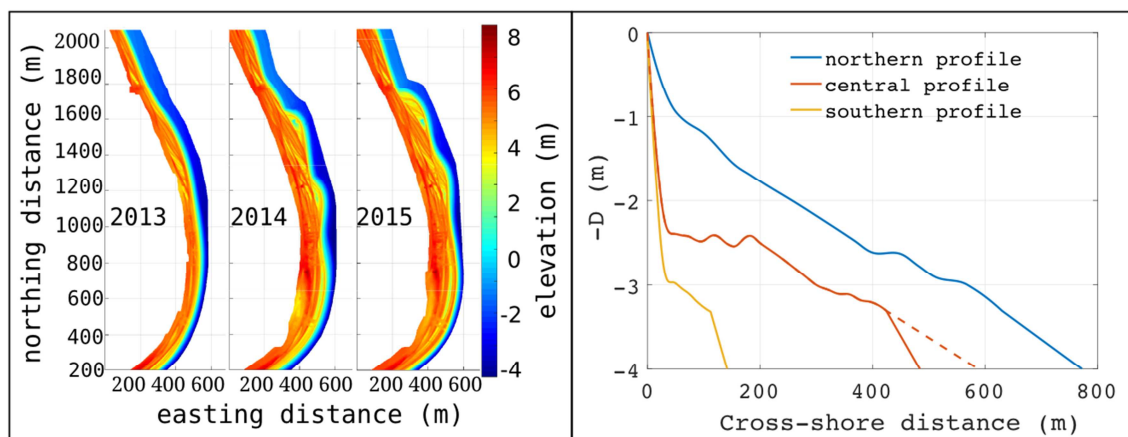

Figure 2. Intertidal topographies of the area of interest showing the initial development of the undulations and the migration towards the north (left) and the profiles along the area of interest (right), the central profile information is chosen for the simulations. After 3.2 m depth the profile information has to be inferred, profile 1 (solid line) assumes a linear decay to the 10-m-depth contour in Figure 3 while profile 2 (dashed line) assumes that the slope is maintained.

The role of high-angle waves, hence shoreline instability associated to alongshore wave-driven sediment transport, on the formation and dynamics of the shoreline undulations was examined via an "energy" ratio, $R = E_{SW}/E_{NE}$. Here the "energy" was computed by integrating $H^{5/2}$ with respect to time for wave angles between $135°−315°$ for SW waves and between $-45°−135°$ for NE waves. The R ratio was computed for the time intervals between shoreline surveys, thus quantifying the degree of dominance of SW waves over NE waves (high-angle waves versus low-angle waves) before every survey. The result showed that the undulations would form during time periods where the SW wave energy was dominant (at least 30 times larger) and they would decay when this dominance was weakened.

3. Wave transformation

3.1. *Wave model equations and setup*

We use the wave module of the morphodynamic Q2D-morfo model (Arriaga et al., 2017b) to propagate the waves from the deep water buoy to a location in front of the undulations, which takes into account refraction and shoaling over the curvilinear contours. It assumes monochromatic waves characterized by T (peak period), H (root-mean-square wave height) and θ (wave angle with respect to the shore normal). The waves are propagated from the offshore boundary, where they are assumed to be uniform, by solving in cascade a set of three decoupled equations: the dispersion relation (Equation 1), the equation for wave number irrotationality (Equation 2) and the wave energy conservation equation (Equation 3).

$$\omega^2 = gk \tanh(kD) \tag{1}$$

$$\frac{\partial k_y}{\partial x} = \frac{\partial k_x}{\partial y} \tag{2}$$

$$\frac{\partial}{\partial x}\left(c_g H^2 \frac{k_x}{k}\right) + \frac{\partial}{\partial y}\left(c_g H^2 \frac{k_y}{k}\right) = 0 \tag{3}$$

Here, ω is the radian frequency, g is the gravity acceleration, $\vec{k} = (k_x, k_y) = k(-\cos\theta, \sin\theta)$ the wave number vector, c_g the group celerity, and D the local depth. These equations ignore wave diffraction, and wave energy dissipation by bottom shear stress and wave breaking.

The large-scale bathymetry across which the waves are propagated is extracted from the General Bathymetric Chart of the Oceans (GEBCO) which redirects the download request to the British Oceanographic Data Center supported by the Natural Environment Research Council. The data correspond to the UTM zone 31U. They are given in degrees and we transform them to UTM coordinates (easting and northing). The final data has a resolution of about 0.5/1.0 km in the Northing/Easting directions (Figure 3).
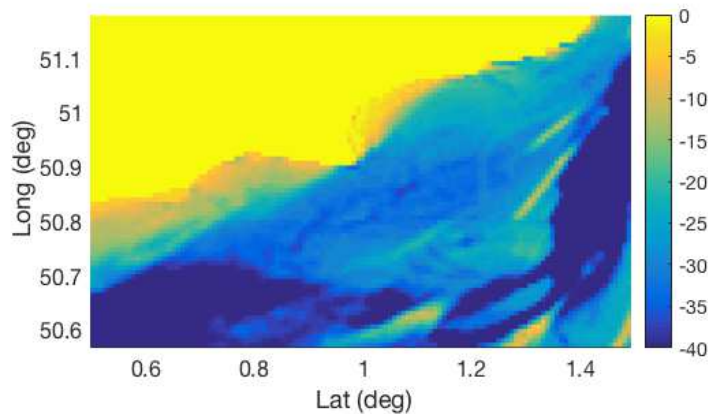

Figure 3. Bathymetry extracted from the General Bathymetric Chart of the Oceans. The dry beach is set to zero for visualization.

3.2. *Resulting waves propagated at 4 m-depth*

The wave characteristics are extracted directly in front of the undulations from the wave field computed across the full large-scale bathymetry, for the SW mean wave conditions and for the NE mean wave conditions. Figure 4 shows the wave angle (with respect to the shore normal at the area of the undulations) and the wave height at 4, 5, and 6 m depth for both the SW waves (top figure) and the NE waves (bottom figure). The alongshore coordinate 0 is near the tip of the cuspate foreland. The NE waves are more

energetic than the SW waves (despite the opposite occurs in deep water), which is indicative of how much the SW waves have refracted. The SW wave height decays in the alongshore direction (i.e., away from the tip) and they are still very oblique even at 4 m depth. Notice also that at the alongshore coordinates 800-2000 m the wave height is constant from 6 to 4 m depth due to the foreland shape. The NE waves show a more regular alongshore behaviour.
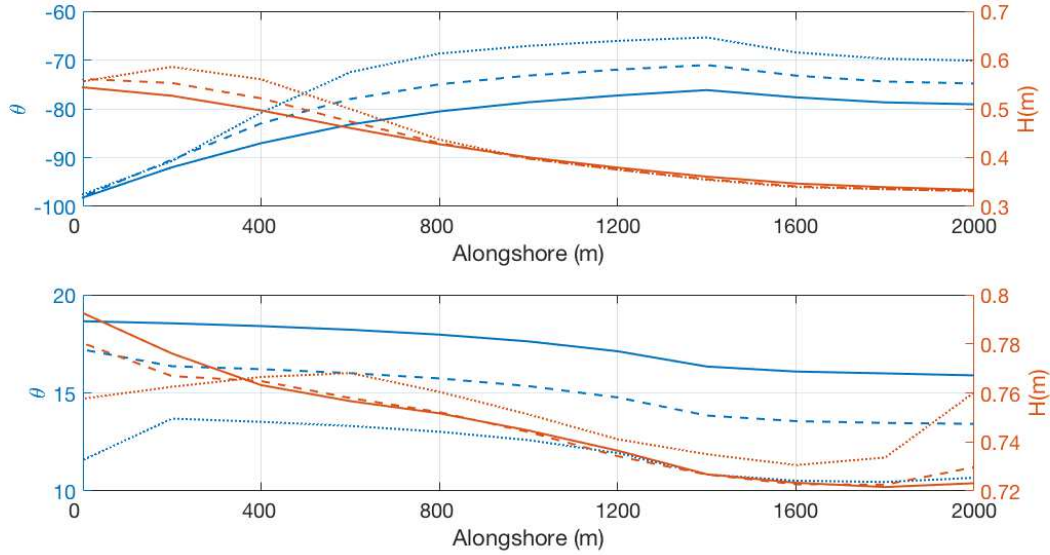

Figure 4. Wave characteristics of SW waves (top) and NE waves (bottom) at depths of 6 m (solid lines), 5 m (dashed lines), and 4 m (dotted lines). The angles are shown with respect to the shore-normal in the area of the undulations.

4. Linear stability analysis

4.1 Model equations and setup

To investigate whether shoreline sand waves can emerge from a morphodynamic instability, a linear stability analysis (LSA) is performed with the 1D-morfo model described in Falqués et al. (2005). The main concepts of the model are as follows. A small undulation is imposed on an initially rectilinear shoreline being defined as:

$$y_s(x,t) = \frac{A}{2} e^{\sigma t + iKx} + c.c. \tag{4}$$

with x, y being Cartesian coordinates in the alongshore and cross-shore directions (respectively), t the time, K the alongshore wavenumber ($L = 2\pi/K$) and $\sigma = \sigma_r + i\sigma_i$ the complex growth rate. Regarding the unperturbed state, the main inputs of the model are the cross-shore beach profile and the significant wave height, peak period and angle at a certain depth. Regarding the perturbation, the main inputs are its alongshore wavelength, L, its cross-shore shape and the depth of its offshore reach, D_c.

To compute the growth rate, equation (4) is inserted into the one-line sediment conservation equation:

$$\frac{\partial y_s}{\partial t} = -\frac{1}{\overline{D}} \frac{\partial Q}{\partial x} \tag{5}$$

where $\overline{D}$ is a mean depth of the morphodynamic active zone and Q is the total alongshore sediment transport rate. Here, Q is computed with the CERC formula:

$$Q = \mu H_b^{5/2} \sin 2\alpha_B \tag{6}$$

where H_b, α_b are the wave height and wave angle with respect to the local shore normal at breaking and μ is an empirical constant. In the present contribution it is set to $\mu = 0.15 \text{ m}^{1/2}\,\text{s}^{-1}$.

Computing the left hand side of Equation (5) is straightforward from Equation (4) but estimating the right hand side requires calculating the perturbed H_b and α_b. This is done by linearizing (with respect to A) the equations describing refraction and shoaling over the perturbed bathymetry (Equations 1-3) and computing H_b and α_b numerically.

The model setup requires an equilibrium profile, a shape of the profile perturbation and a value of the depth of closure. The first one is extracted from the high-resolution intertidal topographic surveys (which extend to about 3 m depth) and the bed level beyond these measurements is inferred from the 10 m depth contour of the large-scale bathymetry used to propagate the waves. Two equilibrium profiles are in fact used, corresponding to two different manners to extrapolate the detailed survey up to 4 m depth (Figure 2, right). In profile 1, the extrapolation is performed assuming a linear decay from 3 m to the 10-m-depth contour. In profile 2, we simply assume that the slope at 3 m depth is maintained up to 4 m depth. The default shape of the profile perturbation is a profile shift, which is reasonable bearing in mind that we use a shallow depth of closure. There are no direct measurements of the depth of closure at this site, a relatively close site where such measurements are available is the South Dutch coast. Hinton and Nicholls (1998) studied the variability of cross-shore profiles over 20 years and found a closure depth of 5 m. In that coast a mega-nourishment (ZandMotor) was recently constructed and measurements over 3 years show a noticeable variability at 8 or 9 m depth, suggesting a larger depth of closure (Arriaga et al., 2017b). In the present work, we decided to use a default depth of closure of 4 m in front of Dungeness for two reasons. The first one is based on the observations: the waves are less energetic than at the southern Dutch coast and the Dungeness shoreline undulations are much smaller features than the ZandMotor. The second reason results from a model limitation: the 1Dmorfo model assumes alongshore-uniform unperturbed depth contours parallel to the shoreline while the contours at the northern flank of the Dungeness Foreland show a Spanish fan shape (i.e., the bathymetric contour orientation gradually approaches the shoreline orientation and can be seen as a slope change of the cross-shore profiles in Figure 2). Then, if a larger depth of closure is used, the 1Dmorfo wave propagation does not represent well the real propagation at this site. The offshore wave conditions (*H, T, θ*) we use correspond to the values propagated at the chosen depth of closure of 4 m (see section 3). We only take one value for the wave height, one value for the peak period, and a wave incidence range of 10° due to its alongshore variability $H_{SW} = 0.4\ m$, $T_{SW} = 6.8\ s$, $\theta_{SW} = 70^o - 80^o$, $H_{NE} = 0.73\ m$, $T_{NE} = 5.5\ s$, $\theta_{NE} = 0^o - 10^o$ (Figure 4).

4.2 Results

Figure 4 shows the growth rate obtained for wavelengths in the range 150-1000 m. Smaller wavelengths are not consistent with the 1D-model model assumption that wavelengths must be much larger than the surf zone width (which is about 10 m for the mean SW waves). Larger wavelengths always have negative growth rates. As can be seen in Figure 4, the NE waves are predicted to dampen the undulations (negative growth rates) for every wavelength while the SW waves have the potential to make several wavelengths grow (positive growth rates). The magnitude of the growth rate induced by the NE waves is one order of magnitude larger than the growth rate induced by the SW waves. When using profile 1, two wavelengths are predicted to emerge for an angle of 80°: 210 m and 410 m (190 m and 390 m for 70°), the fastest growing one corresponding to the smallest wavelength. For profile 2, several wavelengths are predicted to emerge for an angle of 80°: 150 m, 180 m, 300 m, 450 m and 900 m (160 m, 270 m, 390 m and 750 m for 70°), the fastest growing one corresponding to 300 m. In general, smaller incident wave angles produce smaller wavelengths and larger growth rates. Also, for profile 2 the shape of the growth rate curve is more irregular and not as clear as for profile 1. Model runs for a depth of closure of 6 m have also been performed and the growth rates are one order of magnitude smaller than those obtained for a 4 m closure depth. This is due to the unrealistic wave propagation from 6 to 4 m in 1Dmorfo model for this site.
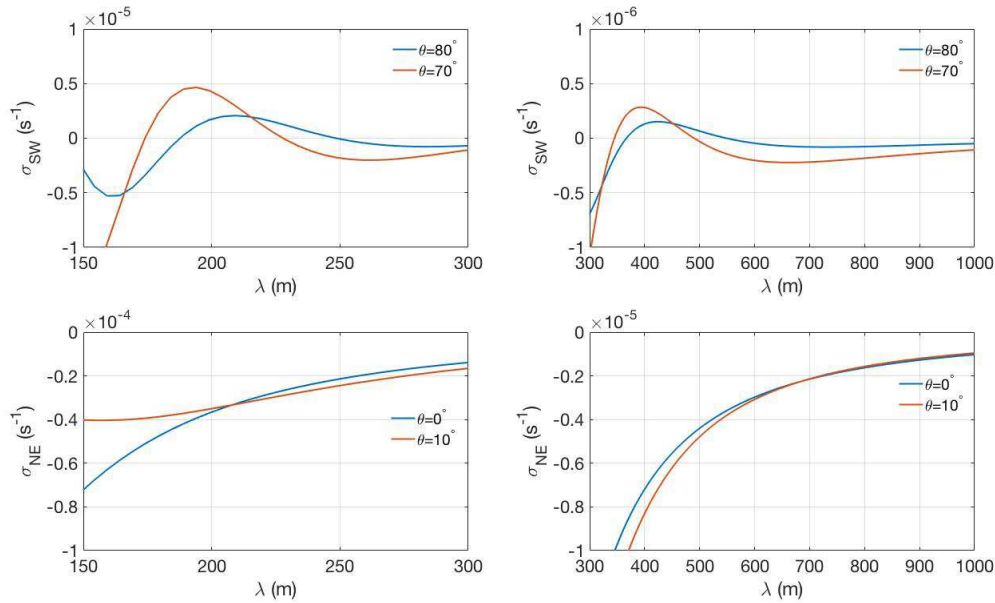
Figure 5. Growth rate for the wavelengths between 150 m and 1000 m induced by the SW waves (top panels) and the NE waves (bottom panels) using profile 1. The left panels correspond to the 150 m-300 m range and the right panels to the 300 m – 1000 m range. The y-axis range is one order of magnitude smaller in the 300 m – 1000 m range.
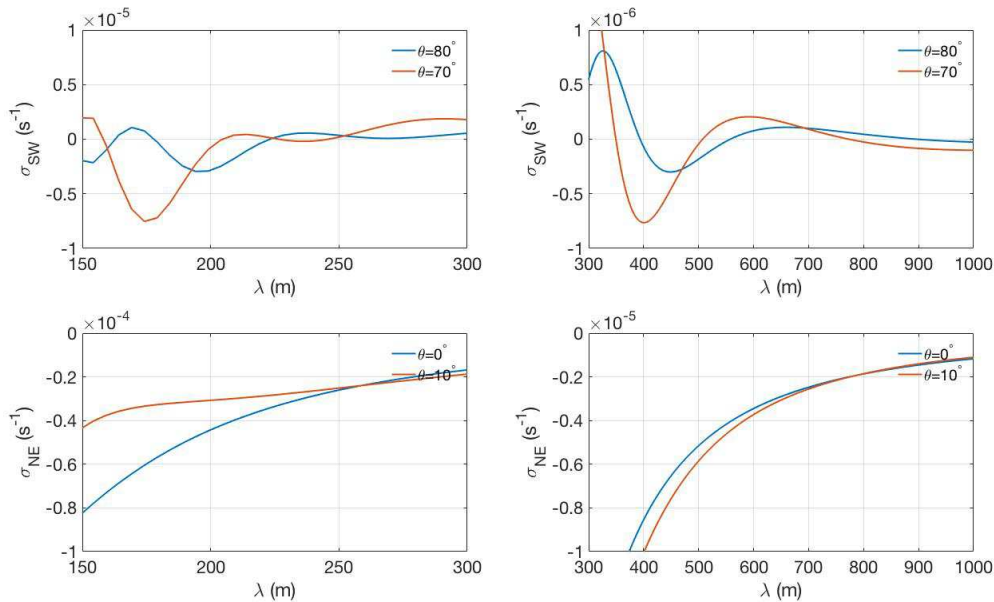

Figure 6. Growth rate for the wavelengths between 150 m and 1000 m induced by the SW waves (top panels) and the NE waves (bottom panels) using profile 2. The left panels correspond to the 150 m-300 m range and the right panels to the 300 m – 1000 m range. The y-axis range is one order of magnitude smaller in the 300 m – 1000 m range.

The growth rate curves for highly-oblique waves display 2 to 4 maxima in the studied range of wavelengths, which does not occur for intermediate angles of incidence (not shown). This behaviour is quite uncommon and was also obtained by Uguccioni et al. (2006) and seems to be related to the high wave

obliquity in shallow waters (4 m depth).

5. Discussion

The linearity of the model equations described in section 4 means that it makes sense to do an average of the growth rates corresponding to the SW and NE waves with certain probability of occurrence (p_*): $\sigma = \sigma_{SW}p_{SW} + \sigma_{NE}p_{NE}$. For the period 2006–2016, p_{SW} is 0.65 and a negative averaged growth rate is then obtained. In fact a p_{SW} of 0.92 is required to obtain positive growth rates, in which case the fastest growing wavelength is of 200 m for the profile 1 (Figure 7), with a growth time of $1/\sigma$=12 d. For profile 2, the same probability gives a growth time of $1/\sigma$=40 d for a wavelength of 300 m. This indicates that a very large percentage of SW waves is required for the undulations to grow, which is consistent with the fact that shoreline undulations of 400 m at Dungeness only appeared after periods of very energetic SW waves (Arriaga et al., 2017a). Notice that in this preliminary analysis we are running the model for mean wave conditions instead of the wave conditions observed before the formation of the undulations. The linear stability analysis should be performed for the specific time periods (previous to the formation of the undulations) using the measured time series of wave conditions instead of mean wave conditions.

The bathymetric perturbation associated to the shoreline undulations is essential for the feedback between waves and morphology leading to the instability. But as the 1Dmorfo model is based in the one-line approximation, the link between shoreline undulations and bathymetric undulations must be prescribed and this is done by selecting a particular shape of the bathymetric perturbation. The influence of this choice has been investigated thoroughly by Idier et al. (2017). This research showed that low-angle waves can also be de-stabilizing in case of a bed level perturbation with a linear decay from the shoreline to the depth of closure. We tested this perturbation shape (not shown here) and we found that the NE waves give positive growth rates while the SW waves give negative growth rates for wavelengths in the order of the observed undulations. We therefore conclude that this type of perturbation shape does not properly represent the physics of the instability mechanism in this site.
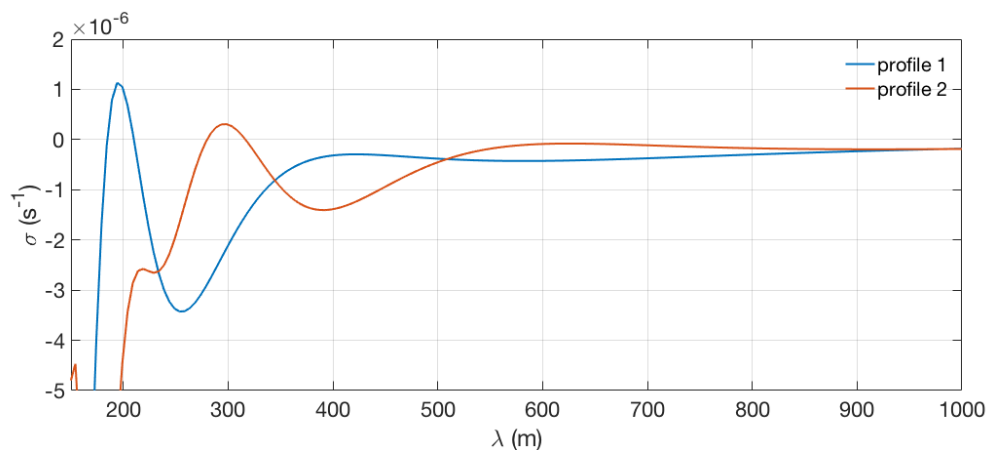

Figure 7. Growth rate combined assuming the 92% of waves coming from the SW and 8% coming from the NE for the two profiles analysed.

An important part of the methodology that can be improved is related to the wave transformation. On the one hand, the wave model used here does not take into account diffraction which may affect the wave transformation, especially because of the cuspate shape and the fact that we need to propagate until shallow depths. On the other hand, the input bathymetry for the model can be improved by combining the low-resolution information (bathymetry used for wave propagation) with the high-resolution information (the intertidal bathymetry). Even though the high-resolution-intertidal topographies arrive to a shallower depth than 4 m, the correct representation of the 3-m contour will give a more accurate interpolation for the area between 3-m and 10-m depth.

Finally, simulations with the Q2Dmorfo model can be done in order to avoid the dependence on the shape perturbation and to overcome the assumptions of the 1Dmorfo model of an infinite shoreline and unperturbed parallel bathymetric contours. The Q2Dmorfo model has proven to work well with irregular shoreline shapes such as the ZandMotor (Arriaga et al., 2017b).

6. Conclusions

Arriaga et al. (2017a) described the formation of shoreline undulations with a wavelength of about 400 m at the northern flank of the Dungeness foreland. The existence of these undulations was correlated with SW waves (high-angle waves with respect to the mean shoreline at this site) dominance over the NE waves (low-angle waves). In the present contribution we have investigated the shoreline stabilizing/destabilizing effect of the SW and NE mean wave conditions. Since the waves are measured at a 43 m depth buoy that is located SW of the cape, the SW waves have been transformed up to the 4 m depth contour in front of the undulations and it is found that they are still very oblique (about an angle of 70°). The mean wave characteristics were used to force the 1Dmorfo model (Linear Stability Analysis) to investigate the role of the HAWI mechanism in the formation of the undulations. A shape of the bathymetric perturbation associated to the sand waves corresponding to a cross-shore profile shift has been selected. It is found that such perturbation is required for the growth of sand waves with the observed characteristics. The SW waves produce positive growth rates while the NE waves produce negative growth rates one order of magnitude larger. The strong refraction until 4 m depth experienced by the SW waves cause them to lose a lot of energy (a wave height decay from 1.4 m to 0.4 m) while the NE waves conserve more energy (a wave height decay from 1.1 m to 0.73 m). Computing the average growth rate by combining the growth rates for both directions, a weighting of 92% for the SW waves (and 8% for the NE waves) is required to have a positive growth rate. This is consistent with the strong observed SW wave dominance during the formation events. In this case the emerging wavelengths are in the range 200−300 m. However, it is difficult to assess whether those weightings are representative of the observed conditions. Future work is required to understand the formation events of the undulations for which we will compute the time series of hourly growth rates as a function of the time series of wave parameters. The correlation between large positive growth rates and sand wave occurrence can then be assessed. Also, a non-linear morphodynamic model such as Q2Dmorfo will be used to study the non-linear regime.

Acknowledgements

References

Arriaga., J, Falqués, A., Ribas, F., Crews, E., 2017a. Observation of formation events of shoreline sand waves on a gravel beach. *Submitted to Ocean Dynamics.*

Arriaga, J., Rutten, J., Ribas, F., Falqués, A., Ruessink, G., 2017b. Modeling the long-term diffusion and feeding capability of a mega-nourishment. *Coastal Engineering,* 121: 1-13.

Ashton, A., Murray, A.B., Arnault, O., 2001. Formation of coastal features by large-scale instabilities induced by high-angle waves. *Nature*, 414: 196-300.

Ashton, A. and Murray, A.B., 2006a. High-angle wave instability and emergent shoreline shapes: 1. Modeling of sand waves, flying spits, and capes.. *Journal of Geophysical Research,* 111. Doi:10.1029/2005JF000,422.

Ashton, A. and Murray, A.B., 2006b. High-angle wave instability and emergent shoreline shapes: 2. Wave climate analysis and comparisons to nature. *Journal of Geophysical Research,* 111. Doi:10.1029/2005JF000,423.

Coco, G., Murray, A.B., 2007. Patterns in the sand: from forcing templates to self-organization. *Geomorphology*, 91: 271-290.

Davidson-Arnott, R.G.D. and van Heyningen, A., 2003. Migration and sedimentology of longshore sandwaves, Long Point, Lake Erie, Canada. *Sedimentology*, 50: 1123-1137.

Dornbusch, U., 2005. BAR phase 1, beach material properties. *Technical Report.* University of Sussex.

Falqués, A. and Calvete, D., 2005. Large scale dynamics of sandy coastlines. Diffusivity and instability. *Journal of Geophysical Research,* 110. Doi:10.1029/2004JC002587.

Green, R.D., 1968. Soils of Romney Marsh. *Soil survey of Great Britain*, Bulletin 4.

Hinton, C. and Nicholls, R.J., 1998. Spatial and temporal behaviour of depth of closure along the Holland coast. *Proceedings of the 26th International Conference of Coastal Engineering.* doi*:*10.1061/9780784404119.221.

Idier, D., Falqués, A., Rohmer, J., Arriaga., J., 2017. Self-organized kilometre-scale shoreline sandwave generation: sensitivity to model and physical parameters. *Submitted to Journal of Geophysical Resarch –Earth Surface.*

Kaergaard, K., Fredsoe, J., Knudsen, S.B., 2012. Coastline undulations on the West Coast of Denmark: Offshore extent, relation to breaker bars and transported sediment volume. *Coastal Engineering,* 60: 109-122.

Long, A.J., Waller, M.P., Plater, A.J., 2006. Coastal resilience and late Holocene tidal inlet history: The evolution of Dungeness Foreland and the Romney Marsh depositional complex (U.K.). *Geomorphology,* 82(3-4): 309-330.

Medellín, G., Medina, R., Falqués, A., González, M., 2008. Coastline sand waves on a low-energy beach at 'El Puntal' spit, Spain. *Marine Geology,* 250: 143-156.

Ribas, F., Falqués, A., de Swart, H.E., Dodd, N., Garnier, R., Calvete, D., 2015. Understanding coastal morphodynamic patterns from depth-averaged sediment concentration. *Rev. Geophys.,* 53. Doi:10.1002/2014Rg000457.

Ryabchuk, D., Leont'yev, I., Sergeev, A., Nesterova, E., Sukhacheva, L., Zhamoida, V., 2011. The morphology of sand spits and the genesis of longshore sand waves on the coast of the eastern Gulf of Finland. *Baltica,* 24(1): 13-24.

Uguccioni, L., Deigaard, R., Fredsoe, J., 2006. Instability of a coastline with very oblique wave incidence. *Proceedings of the 30th International Conference of Coastal Engineering Conference,* 1(5): 3542-3553.

van den Berg, N., Falqués, A., Ribas, F., 2012. Modelling large scale shoreline sand waves under oblique wave incidence. *Jounral of Geophysical Research,* 117. Doi:10.1029/2011JF002177.

Verhagen, H.J., 1989. Sand waves along the Dutch coast. *Coastal Engineering,* 13: 129-147.